PERGAMON

International Journal of Plasticity 19 (2003) 2083–2098

INTERNATIONAL JOURNAL OF Plasticity

www.elsevier.com/locate/ijplas

Elasto-plasticity of paper

Jaime Castro[a,*], Martin Ostoja-Starzewski[b]

[a]*Institute of Paper Science and Technology, 500 10th Street, N.W., Atlanta, GA 30318-5794, USA*

[b]*Department of Mechanical Engineering, McGill University, 817 Sherbrooke Street West, Montreal, Quebec, Canada H3A 2K6*

Received in revised form 4 February 2003

Abstract

We develop a constitutive model of paper's in-plane biaxial tensile response accounting for the elastic–plastic hardening behavior, and its orthotropic character. The latter aspect is motivated by machine-made papers, which, in contrast to isotropic laboratory handsheets, are strongly oriented. We focus on modeling paper's response under monotonic loading, this restriction allowing us to treat the elastic-plastic response as a physically nonlinear elastic one. A strain energy function of a hyperbolic tangent form is developed so as to fit the entire range of biaxial and uniaxial experiments on a commercial grade paper. This function may then be introduced as the free energy function into a model based on thermomechanics with internal variables.

Keywords: Elasto-plasticity; Nonlinear elasticity; Thermomechanics

1. Background

Paper displays various unconventional mechanical properties both below and beyond the plastic limit, all the way up to its failure. These properties—especially in the simplest case of elastic response—have been studied over the past half a century by experiments, mechanics analyses and, more recently, by ever more complex computer simulations of cellulose fiber microstructures making up paper; see (Deng and Dodson, 1994; Niskanen, 1998; Bronkhorst and Bennett, 2001) for reviews. In this report we shall focus on paper's in-plane tensile response for specimens on

* Corresponding author.

0749-6419/03/$ - see front matter © 2003 Published by Elsevier Ltd.
doi:10.1016/S0749-6419(03)00060-3

length scales of several centimeters, and will not concern ourselves with very different (buckling-type) response in compression. Another restriction will involve a disregard of viscosity, which is justified by the low strain rate values of interest, and which—in contradistinction to most other materials—is controlled by humidity much more than by temperature. However, an important challenge not to be omitted here concerns modeling paper's response with due account of its orthotropy—both in the linear elastic and nonlinear plastic ranges. Orthotropy is very important for machine made paper as opposed to isotropic laboratory made handsheets.

As is well known (see reviews by Niskanen, 1993, 1998), there is an approximately linear section at small strains in the load-elongation curve of paper. Nevertheless, the yield point has no unique definition because the deviation from the linear portion grows gradually as elongation increases. Thus, one way to define the yield point is to identify stress (and strain) at which the smooth curve begins to deviate from straight line beyond a certain percentage. Another way to find a yield point in paper is through loading and unloading to determine the deviation point from elastic linearity, but, as seen in Fig. 1, not even for small strains, is this universally possible. Considering that no precise yield point can be identified unequivocally, the hyperbolic tangent function of the hyperelastic model originally due to Johnson and Urbanik (1984), Suhling et al. (1989), and Suhling (1990) is an attractive starting point for modeling paper behavior.

In the aforementioned research an approximate form of the strain energy function $w(\varepsilon)$, $\varepsilon(\equiv\varepsilon_{ij})$ being strain, was found empirically by strongly compromising between experimental data from biaxial tests and uniaxial tests in the machine direction (MD or x_1) and cross direction (CD or x_2). We will try to come up with a better analytical fit to $w(\varepsilon)$ employing our own experiments on commercial grade paper over the range from uniaxial MD, through biaxial MD–CD, up to uniaxial CD loadings. In this paper we use a symbolic ($\mathbf{t}$) or an indicial ($t_{ij...}$) notation for a tensor, whichever is more convenient.

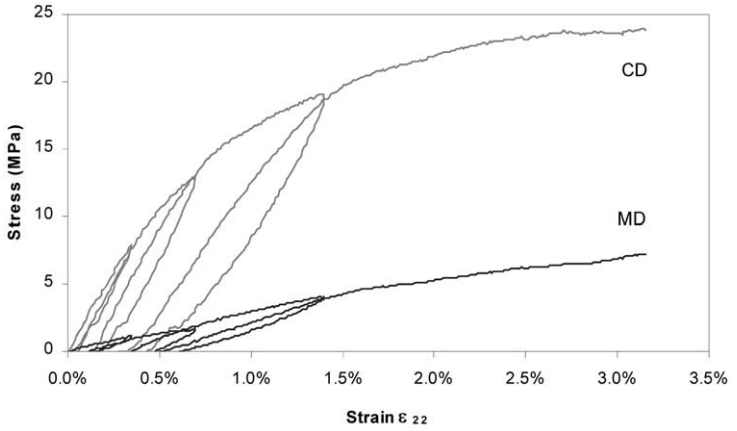

Fig. 1. Stress–strain curve for case (0.0, 1.0) in biaxial cyclic loading and unloading.

The hyperelastic function $w(\varepsilon)$ may model paper's behavior under monotonic loading as a nonlinear elastic material equivalent to the actual plastic one, but it cannot describe the plastic unloading. However, $w(\varepsilon)$ may then be introduced as the free energy function in a model based on thermomechanics with internal variables, while also a dissipation function is introduced to deal with the irreversible effects. This, in fact, is the approach recommended at the end of our paper, while following the *thermomechanics with internal variables* (T.I.V.) developed by Ziegler (1983); see also (Germain et al., 1983), Maugin, 1992; 1999), Collins and Houlsby (1997), Houlsby and Puzrin (2000) and (Aboudi et al., 2003) among others. Finally we note that T.I.V. lends itself to a generalization to randomly heterogeneous media as shown in (Ostoja-Starzewski, 2002), and thus holds promise for handling random (spatial) formation and associated scale effects in paper (Ostoja-Starzewski and Castro, in press).

2. Paper as an elastic–plastic orthotropic material

2.1. Experiments

Material specimens selected for testing in uniaxial and biaxial tests were cut from commercial grade paper sheets of *white textured Crayola sketchpaper*. This paper had nominal thickness of about 136 μm, mass density $\rho = 508$ kg/m^3, and hence 'grammage' (or 'basis weight,' i.e. weight per unit area in plane of paper)of about70 g/m^2. The specimens were of size 145 × 145 mm. The uniaxial MD and CD standard tests (Tappi T-494) were performed in an Instron tensile tester on paper samples preconditioned at 23 °C, 20% relative humidity (R.H.); they were then conditioned and tested at 23 °C, 20% R.H. (Tappi Standard T-402). In the biaxial tests (Fig. 2), the paper samples were also preconditioned at 23 °C, 20% R.H., but were not tested at the same standard conditions. Fig. 3 compares the stress–strain curves from uniaxial standard tests in MD and CD carried out on the Instron and the biaxial tester. This comparison shows that the results are consistent despite the difference in ambient conditions.

Figs. 4 and 5 shows stress–strain curves of the 145 × 145 mm paper coupons under different uniform displacement boundary conditions. All four clamps are semi-rigid along their length. Eleven combinations of MD-CD strain rates were considered according to the list in Table 1; we employ here the convention: $(\varepsilon_{11}, \varepsilon_{22})$.

Fig. 6 shows the equivalent curves for all the loading cases, now displayed in the stress plane. The average elastic moduli from these tests were rounded to $E_1 = 4400$ MPa in MD and to $E_2 = 2200$ MPa in CD. Also from the curves of Figs. 4 and 5, the yield stress was approximated to 20 MPa and 10 MPa in MD and CD, respectively. On the other hand, biaxial tests made it possible to estimate Poisson's ratios: ν_{12} was determined equal to 0.20 from the loading case (1.0, 0.0), while ν_{21} was found equal to 0.10 from case (0.0, 1.0).

The biaxial data also provides the means to approximately determine the yield surface and failure envelope as shown in Fig. 7. The approximation of yield surface

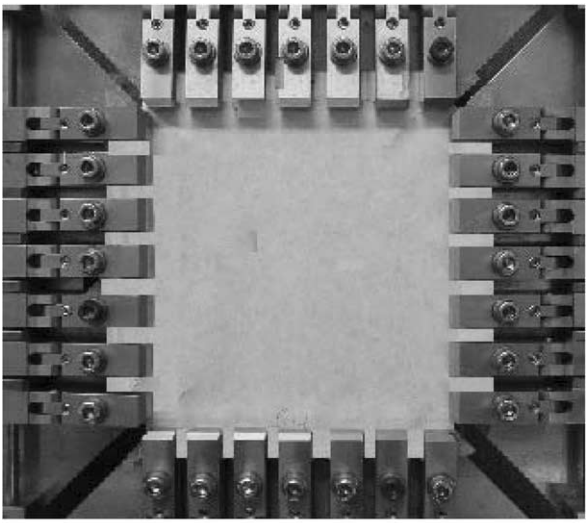

Fig. 2. Biaxial testing setup with a square-shaped paper specimen clamped at its edges.

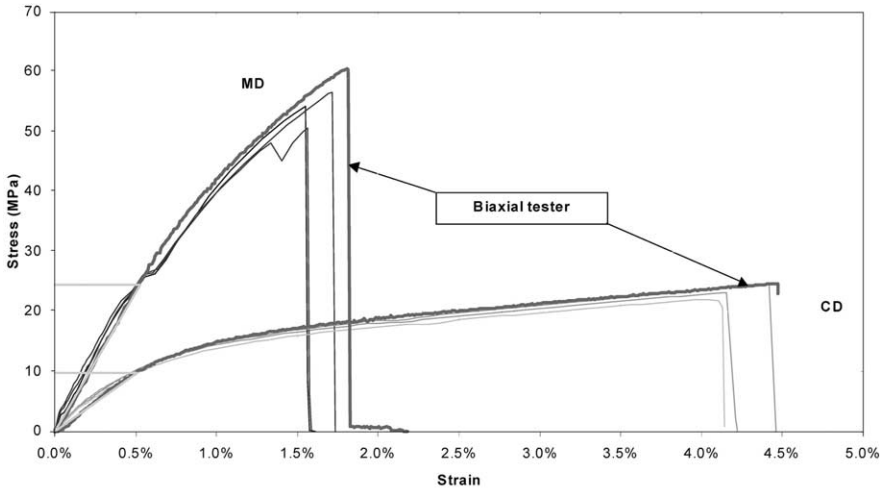

Fig. 3. Typical stress–strain curves in uniaxial loadings in MD and CD.

is due to the somewhat indefinite nature of the yield point (σ_Y) as already discussed in the Background section, and, based on our measurements, we propose a condition in terms of maximum normal stresses in coordinates aligned with material directions MD and CD, augmented by a similar statement for the shear stress

$$\sigma_{11} \leqslant \sigma_{11,Y} \qquad \sigma_{22} \leqslant \sigma_{22,Y} \qquad \sigma_{12} \leqslant \sigma_{12,Y} \tag{1}$$

An experimental test of plastic response of paper under shear—and thus, a precise determination of the $\sigma_{12,Y}$ value—is very unwieldy. In most paper physics literature

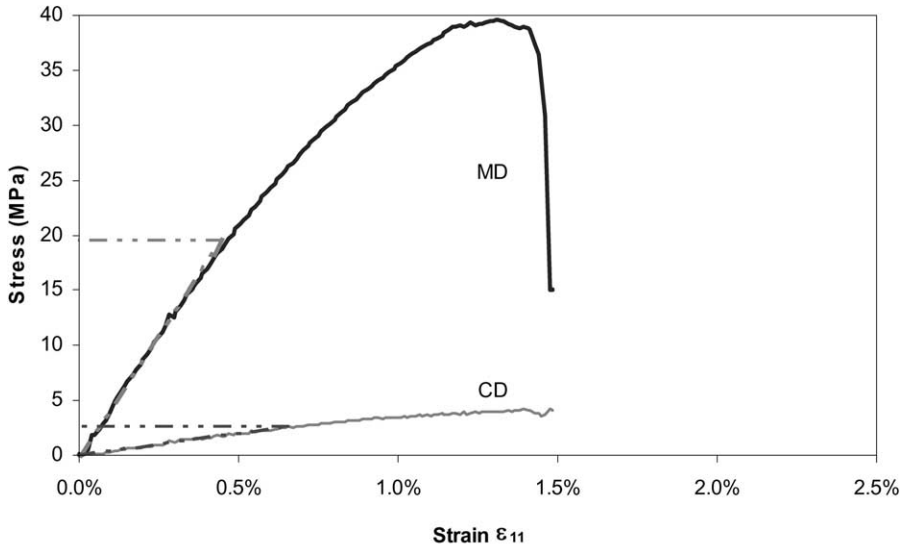

Fig. 4. Stress–strain curves case (1.0, 0.0); recall Table 1.

Table 1
Loading cases under uniform displacement b.c

Loading case	MD (X-axis)	CD (Y-axis)
(1.0, −0.2)	0.5 mm/s	−0.1 mm/s
(1.0, 0.0)	0.5 mm/s	0.0 mm/s
(1.0, 0.2)	0.5 mm/s	0.1 mm/s
(1.0, 0.4)	0.5 mm/s	0.2 mm/s
(1.0, 0.6)	0.5 mm/s	0.3 mm/s
(1.0, 1.0)	0.5 mm/s	0.5 mm/s
(0.6, 1.0)	0.3 mm/s	0.5 mm/s
(0.4, 1.0)	0.2 mm/s	0.5 mm/s
(0.2, 1.0)	0.1 mm/s	0.5 mm/s
(0.1, 1.0)	0.05 mm/s	0.5 mm/s
(0.0, 1.0)	0.00 mm/s	0.5 mm/s

an elliptical yield condition (e.g. Bronkhorst and Bennett, 2001) is more popular.

The approximation of failure envelope is due to a rather strong random scatter of failure from one specimen to another—all being nominally the same. This envelope can roughly be approximated by the tensorial relationship specialized to plane stress, so that we have an ellipse

$$F_{11}\sigma_{11}^2 + 2F_{12}\sigma_{11}\sigma_{22} + F_{22}\sigma_{22}^2 + F_{66}\sigma_{12}^2 = 1. \tag{2}$$

Excepting F_{12}, the coefficients in Eq. (2) can be approximated by the following expressions:

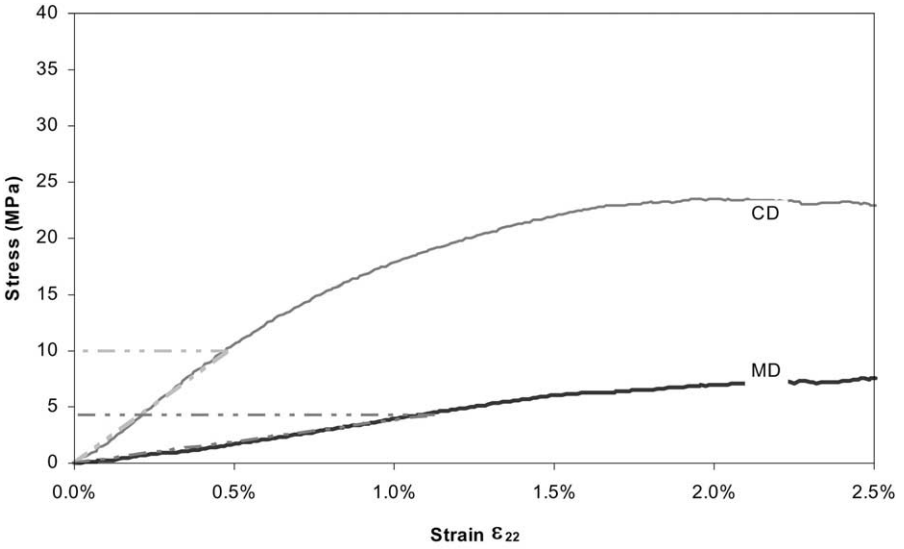

Fig. 5. Stress–strain curves case (0.0, 1.0); recall Table 1.

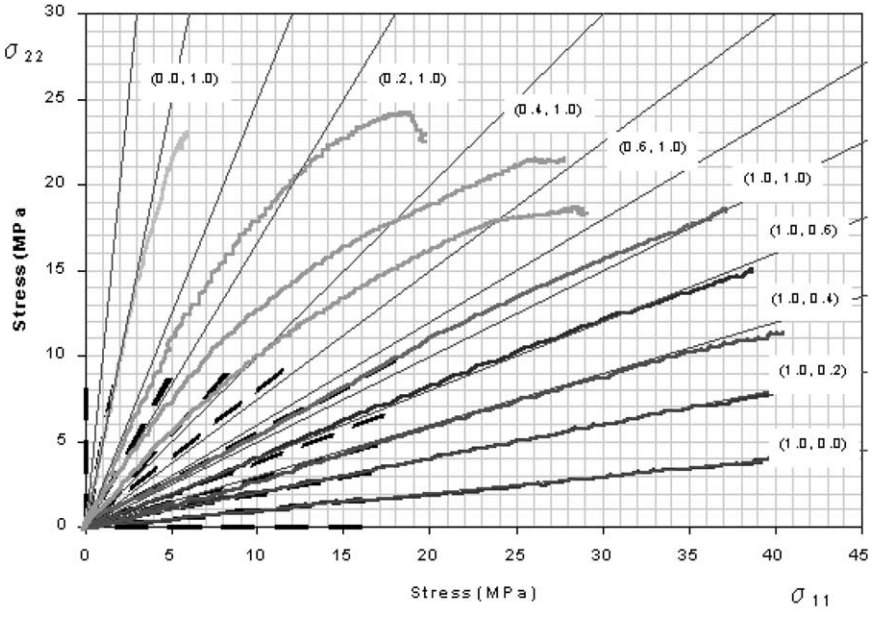

Fig. 6. Biaxial responses in several loading cases; recall Table 1. Solid lines are experimental curves and dashed lines are predictions of the linear elastic orthotropic model (5–7) up to the yield point.

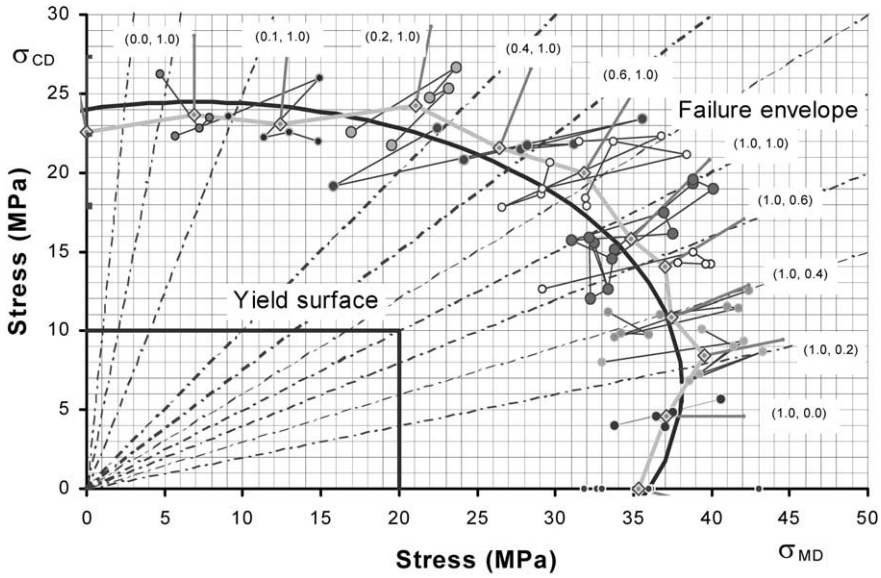

Fig. 7. Yield surface and random failure enevlope of paper. Points of failure having the same loading designation are joined segments, and marked by the same color.

$$F_{11} = \frac{1}{XX'} \qquad F_{22} = \frac{1}{YY'} \qquad F_{66} = \frac{1}{S^2}, \tag{3}$$

where, X, X', Y, and Y' are the tensile and compressive strengths in MD and CD, respectively, and S is the pure shear strength. The following values, all in MPa, give the elliptical failure surface shown in Fig. 7 when $F_{12} = 0$

$$X = 36 \qquad X' = 22 \qquad Y = 24 \qquad Y' = 11 \qquad S = 15. \tag{4}$$

Finally we report that the mechanical properties were also measured with the ultrasonic testing devices at IPST. These measurements were $E_1 = 5.5$ GPa, $E_2 = 2.12$ GPa, $G = 1.32$ GPa, $\rho_{12} = 0.18$, and $\rho_{21} = 0.46$. As expected from paper physics (see Baum et al., 1983), the MD- (respectively, CD-) elastic modulus from the ultrasound measurement is larger (smaller) than the one measured mechanically.

2.2. Linear elastic orthotropic model

The linear elastic, orthotropic behavior of paper prior to yielding can be modeled by the classical model (see e.g. Uesaka et al., 1979)

$$\sigma_{11} = \frac{E_1}{(1 - \nu_{12}\nu_{21})}\varepsilon_{11} + \frac{E_2\nu_{12}}{(1 - \nu_{12}\nu_{21})}\varepsilon_{22} \tag{5}$$

$$\sigma_{22} = \frac{E_1 \nu_{21}}{(1 - \nu_{12}\nu_{21})}\varepsilon_{11} + \frac{E_2}{(1 - \nu_{12}\nu_{21})}\varepsilon_{22} \tag{6}$$

$$\tau_{12} = G\gamma_{12} = 2G\varepsilon_{12}, \tag{7}$$

where the engineering constants are: E_1 = Young's modulus in x_1-direction (MD), E_2 = Young's modulus in x_2-direction (CD), $\nu_{12} = \frac{-\varepsilon_{22}}{\varepsilon_{11}}$ is the Poisson's ratio for strain in x_2-direction (CD) when paper is stressed in x_1-direction (MD) only, $\nu_{21} = \frac{-\varepsilon_{11}}{\varepsilon_{22}}$ is the Poisson's ratio for strain in x_1-direction (MD) when paper is stressed in x_2-direction (CD) only, G = shear modulus in x_1x_2-plane.

Here the same constant of proportionality between elastic moduli E_1 and E_2, and Poisson's ratios ν_{12} and ν_{21} is required so as to ensure that the stiffness matrix is orthotropic:

$$\frac{E_1}{E_2} = \frac{\nu_{12}}{\nu_{21}} \quad \text{or} \quad E_1\nu_{21} = E_2\nu_{12}. \tag{8}$$

Now, the shear modulus G can be approximated using the relation proposed by Campbell (1961):

$$G = \frac{E_1 E_2}{E_2 + E_1 + E_1\nu_{21} + E_2\nu_{12}}. \tag{9}$$

This equation expresses the invariance of shear modulus with respect to rotations of the coordinate system—a special property that is approximately satisfied by many paper materials. As an aside, we note that an explanation of this property from the standpoint of micromechanics of random fiber networks was given in (Ostoja-Starzewski and Stahl, 2001).

Now, for the loading case (1.0, 0.0), the strain rate in CD is zero ($\varepsilon_{22} = 0$); by analogy, the strain rate in MD is zero in the loading case (0.0, 1.0). Thus, from (6) and (5) on one hand, and from (5) by (6) on the other hand, we get

$$\frac{\sigma_{22}}{\sigma_{11}} = \nu_{21} \quad \frac{\sigma_{11}}{\sigma_{22}} = \nu_{12}. \tag{10}$$

Using Fig. 4, we find $\nu_{21} = 0.10$, which value is fairly constant up to failure, although the slope decreases with loading. We also find $\nu_{12} = 0.20$. In general, the behavior of curves in that figure is linear when the MD strain rate is dominant [cases (1.0, 0.0) to (1.0, 0.6)], while the nonlinearity of the curves is evident when the CD strain rate is dominant [cases (0.0, 0.6) to (0.0, 1.0)]. With the above values, we find $G = 1294$ MPa from Eq. (9).

Using the determined values of Poisson's ratios and the value for G from Eq. (9), the orthotropic model [Eqs. (5)–(7)] for a homogeneous material gives the dashed

lines shown in Fig. 5 for each loading case. Again, the agreement with the experimental curves is better in the range where MD-strain rate dominates, than in the range where CD-strain rate dominates.

2.3. Nonlinear hyperelastic orthotropic model

2.3.1. Basic framework

We proceed along the lines of hyperelasticity models of paper due to Johnson and Urbanik (1984) who formulated a nonlinear elastic plate model using basic equations of nonlinear elasticity and arrived at a set of constitutive relations which links the plate behavior to its strain energy density $w(e)$. In essence, the model is given by:

$$\sigma_{ij} = \frac{\partial w(e)}{\partial \varepsilon_{ij}}, \tag{11}$$

where, w is a function of the effective strain e which is defined as:

$$e = \frac{\varepsilon_{11}^2}{\nu_{21}} + \frac{\varepsilon_{22}^2}{\nu_{12}} + 2\varepsilon_{11}\varepsilon_{22} + (1 - \nu_{12}\nu_{21})\frac{G}{\nu_{12}E_1}\gamma_{12}^2. \tag{12}$$

The functional form of $w(e)$ had to be found empirically by fitting an assumed function to experiments. Suhling et al. (1989) used a similar empirical approach to determine $w(e)$. In that work, the MD and CD uniaxial stress-strain curves of paperboard were modeled by the expressions:

$$\sigma_{11}(\varepsilon_{11}) = C_1^{MD}\tanh\left(C_2^{MD}\varepsilon_{11}\right) + C_3^{MD}\varepsilon_{11} = \frac{\mathrm{d}w(\varepsilon_{11})}{\mathrm{d}\varepsilon_{11}}, \tag{13}$$

$$\sigma_{22}(\varepsilon_{22}) = C_1^{CD}\tanh\left(C_2^{CD}\varepsilon_{22}\right) + C_3^{CD}\varepsilon_{22} = \frac{\mathrm{d}w(\varepsilon_{22})}{\mathrm{d}\varepsilon_{22}}. \tag{14}$$

These equations could be integrated directly to obtain $w(\varepsilon_{11})$ and $w(\varepsilon_{22})$. Then, by substituting $\varepsilon_{11}(e)$ or $\varepsilon_{22}(e)$, two expressions for $w(e)$ were obtained which, in turn, could be substituted in the following stress–strain relation for a hyperelastic material subjected to plane stress:

$$\begin{bmatrix} \sigma_{11} \\ \sigma_{22} \\ \tau_{12} \end{bmatrix} = 2\frac{\mathrm{d}w(e)}{\mathrm{d}e}\begin{bmatrix} \frac{1}{\nu_{21}} & 1 & 0 \\ 1 & \frac{1}{\nu_{21}} & 0 \\ 0 & 0 & (1 - \nu_{12}\nu_{21})\frac{G}{\nu_{21}E_1} \end{bmatrix}\begin{bmatrix} \varepsilon_{11} \\ \varepsilon_{22} \\ \gamma_{12} \end{bmatrix}. \tag{15}$$

Since the derivatives of each $w(e)$, obtained from CD or MD respectively, led to differing results, neither of these functions could be used to predict the experimental

data in any direction with good accuracy. The proposed alternative was to fit a compromising curve between two strain energy density functions.

2.3.2. Proposed model

We recall from the Background section that there is no clear yield point in the stress–strain response of paper. We can therefore begin by assuming the stress-strain curve to be fitted with an equation of the following form

$$\frac{\mathrm{d}w(\varepsilon_{11})}{\mathrm{d}\varepsilon_{11}} = \sigma_{11} = A\tanh(b\varepsilon_{11}), \tag{16}$$

where A and b are constants to be determined from the experimental data. By taking steps similar to those in Johnson and Urbanik (1984) and Suhling et al. (1989), the empirical Eq. (16) can be integrated to find the stress energy function w

$$w(\varepsilon_{11}) = \int A\tanh(b\varepsilon_{11})\mathrm{d}\varepsilon_{11} = \frac{A}{b}\log[\cosh(b\varepsilon_{11})], \tag{17}$$

which, in terms of the effective strain e, can be written as

$$w(e) = \frac{A}{b}\log\left[\cosh\left(b\sqrt{\frac{\nu_{21}e}{1-\nu_{12}\nu_{21}}}\right)\right]. \tag{18}$$

In view of Eq. (15), we arrive at

$$\sigma_{11} = \frac{A}{\nu_{21}\sqrt{e}}\sqrt{\frac{\nu_{21}}{(1-\nu_{12}\nu_{21})}}\tanh\left(b\sqrt{\frac{\nu_{21}e}{1-\nu_{12}\nu_{21}}}\right)\varepsilon_{11} + \frac{A}{\sqrt{e}}\sqrt{\frac{\nu_{21}}{(1-\nu_{12}\nu_{21})}}\tanh\left(b\sqrt{\frac{\nu_{21}e}{1-\nu_{12}\nu_{21}}}\right)\varepsilon_{22}, \tag{19}$$

$$\sigma_{22} = \frac{A}{\sqrt{e}}\sqrt{\frac{\nu_{21}}{(1-\nu_{12}\nu_{21})}}\tanh\left(b\sqrt{\frac{\nu_{21}e}{1-\nu_{12}\nu_{21}}}\right)\varepsilon_{11} + \frac{A}{\nu_{12}\sqrt{e}}\sqrt{\frac{\nu_{21}}{(1-\nu_{12}\nu_{21})}}\tanh\left(b\sqrt{\frac{\nu_{21}e}{1-\nu_{12}\nu_{21}}}\right)\varepsilon_{22}, \tag{20}$$

$$\tau_{12} = \frac{A}{\sqrt{e}}\sqrt{\frac{\nu_{21}}{(1-\nu_{12}\nu_{21})}}\tanh\left(b\sqrt{\frac{\nu_{21}e}{1-\nu_{12}\nu_{21}}}\right)(1-\nu_{12}\nu_{21})\frac{G}{\nu_{12}E_1}\gamma_{12} \tag{21}$$

From the biaxial tensile test with $\varepsilon_{22} = 0$ [loading case (1, 0)], and using Figs. 4 and 5, the value of b as well as the zero-strain tangent moduli Q_{11} Q_{22}, Q_{12} can now be estimated. In fact, the latter are

$$Q_{11} = \frac{\mathrm{d}\sigma_{11}^{(1,\ 0)}(0)}{\mathrm{d}\varepsilon_{11}} = \frac{Ab}{(1-\nu_{12}\nu_{21})}\cosh^{-2}(0) = \frac{Ab}{(1-\nu_{12}\nu_{21})}, \tag{22}$$

$$Q_{12} = \frac{\mathrm{d}\sigma_{11}^{(0,\ 1)}(0)}{\mathrm{d}\varepsilon_{22}} = Ab\frac{\sqrt{\nu_{12}\nu_{21}}}{1-\nu_{12}\nu_{21}}\sqrt{\frac{\nu_{21}}{\nu_{12}}}\cosh^{-2}(0) = \frac{Ab\nu_{21}}{(1-\nu_{12}\nu_{21})} = Q_{21}, \tag{23}$$

$$Q_{22} = \frac{d_{22}^{(0,\ 1)}(0)}{\mathrm{d}\varepsilon_{22}} = \frac{Ab}{1-\nu_{12}\nu_{21}}\frac{\nu_{21}}{\nu_{12}}\cosh^{-2}(0) = \frac{Ab}{(1-\nu_{12}\nu_{21})}\frac{\nu_{21}}{\nu_{12}}. \tag{24}$$

Therefore, clearly $E_1 = Ab$. Rearranging the above equations and recalling that relation $E_2\nu_{12} = E_1\nu_{21}$ must be satisfied, it follows that

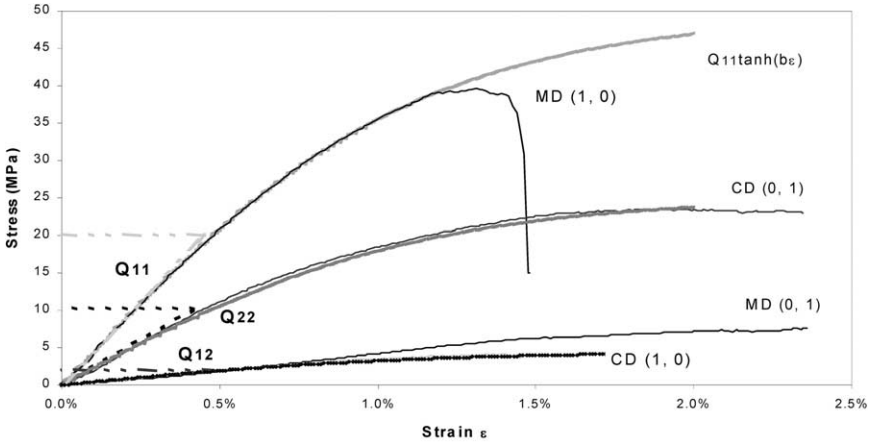

Fig. 8. Fitting of stress–strain curves for loading cases (1.0, 1.0) and (0.0, 1.0).

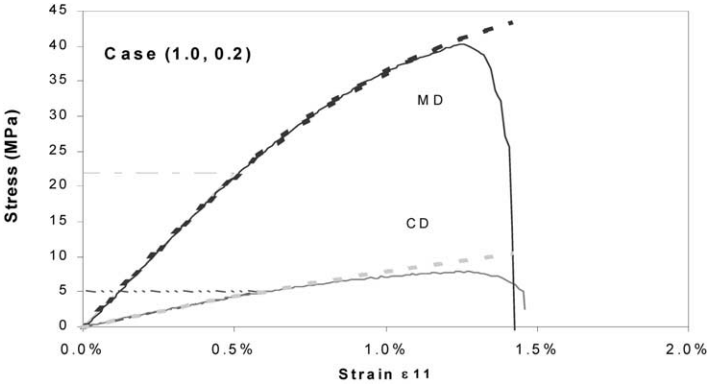

Fig. 9. Fitting of stress–strain curves for loading case (1.0, 0.2). Solid lines are experimental curves and dashed lines are predicted by model (25).

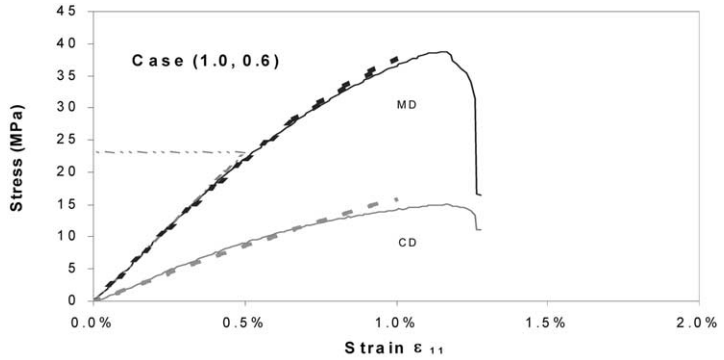

Fig. 10. Fitting of stress–strain curves for loading case (1.0, 0.6). Solid lines are experimental curves and dashed lines are predicted by model (25).

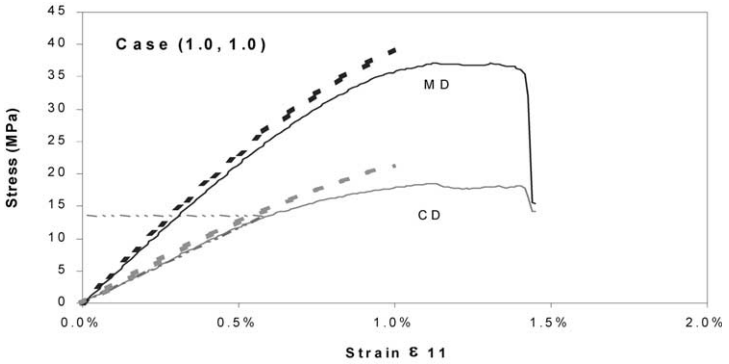

Fig. 11. Fitting of stress–strain curves for loading case (1.0, 1.0). Solid lines are experimental curves and dashed lines are predicted by model (25).

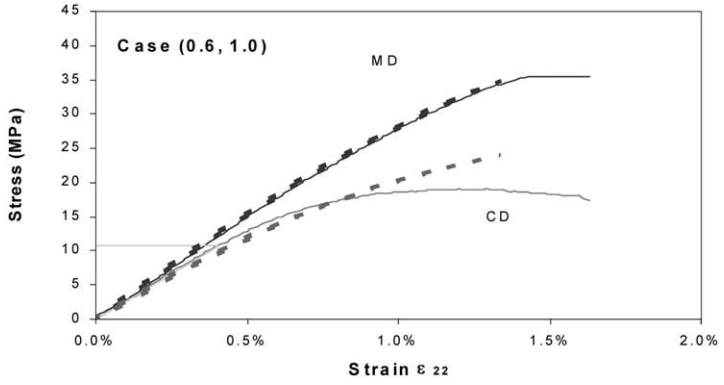

Fig. 12. Fitting of stress–strain curves for loading case (0.6, 1.0). Solid lines are experimental curves and dashed lines are predicted by model (25).

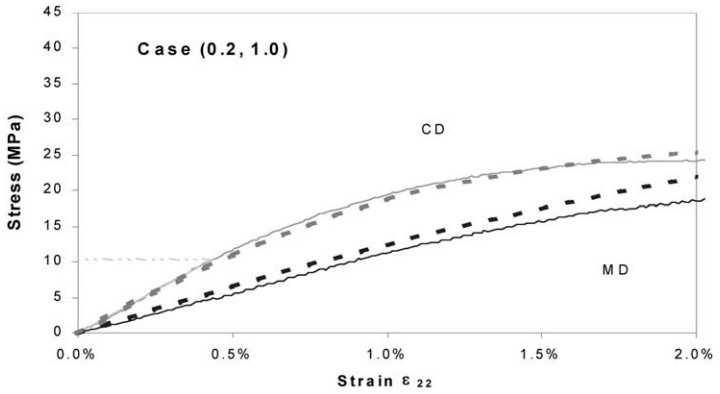

Fig. 13. Fitting of stress–strain curves for loading case (0.2, 1.0). Solid lines are experimental curves and dashed lines are predicted by model (25).

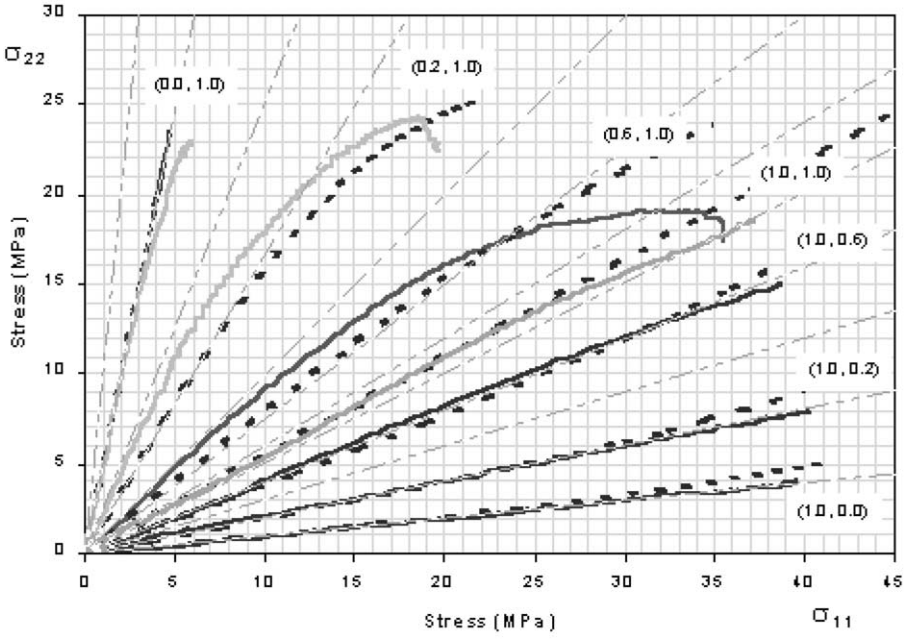

Fig. 14. Several biaxial loading cases. Solid lines are experimental curves and dashed lines are predicted by model (25).

$$\begin{bmatrix} \sigma_{11} \\ \sigma_{22} \\ \tau_{12} \end{bmatrix} = \frac{1}{b} \begin{bmatrix} Q_{11} & Q_{12} & 0 \\ Q_{12} & Q_{22} & 0 \\ 0 & 0 & G \end{bmatrix} \begin{bmatrix} \tanh(b\varepsilon_{11}) \\ \tanh\left(b\sqrt{\frac{\nu_{21}}{\nu_{12}}}\varepsilon_{22}\right) \\ \dfrac{\tanh(b\varepsilon_{11})}{\varepsilon_{11}}\gamma_{12} \end{bmatrix}. \tag{25}$$

It follows that the expression (25) can be derived and fitted with the experimental data from the (1.0, 0) and (0, 1.0) loading cases. Figs. 8–13 show the stress-strain curves predicted by (25) as well as the corresponding experimental curves for various intermediate loading cases. There is an accurate agreement between both curves in general. It can be seen that yielding occurs at about 0.5% strain and that, starting from 0.75% strain, the experimental curve begins to deviate from the predicted (dashed) line. In fact, the occurrence of this deviation was observed to coincide with the appearance of the first cracks, i.e. when damage initiates. A composite picture of all the fits in the stress plane is given in Fig. 14.

For instance, Fig. 8 presents the CD- versus-MD-stress response of the previous loading cases (solid lines are experimental curves and dashed line are predicted curves). Similar to the case of linear elastic orthotropic model, the proposed hyperelastic orthotropic model's agreement with experiments is better in the range where the MD-strain dominates than in the range where the CD-strain dominates.

While the new model does not offer a very good fit for the entire range of strains and/or loading conditions, it is important to note that research on nonlinear hyperelastic models for anisotropic materials in finite strain is beginning only now and is still a formidable challenge in contemporary solid mechanics, e.g. (Dłużewski, 2000).

3. Conclusions

Biaxial tensile tests were performed to obtain stress–strain curves for *white textured Crayola sketch paper* in tension up to failure. These curves allowed us to develop explicit function fits, of hyperbolic tangent type, with a smooth passage from the linear elastic to nonlinear elastic regimes. To the best of our knowledge, these are first constitutive equations of paper consistent for both uniaxial and biaxial loading ranges. Failure surface, including its random scatter, was also mapped by experiments and modeled by an ellipse. The physical origin of inelastic (i.e. plastic-strain-hardening) response is two-fold: (i) pulling out of kinks (microcompressions) and (ii) friction due to the relative movement of microfibrils. Incorporation of these will require inclusion of inelastic effects at the single fiber level in generalizations of network models such as that developed in (Ostoja-Starzewski and Stahl, 2001).

It is well known that, under proportional monotonic loading, effectively strain-hardening elastoplastic composites can be treated in the framework of deformation theory, which is formally equivalent to physically nonlinear, small-deformation elasticity, e.g. (Ponte Castaneda and Suquet, 1998). Thus, a constitutive model of paper, for the biaxial tensile loading regime, treated as an elastic-plastic material with unloading can be developed in either of two ways. First, one can start from the principles of thermomechanics with internal variables, see e.g. (Ziegler and Wehrli, 1987), (Maugin, 1992) or (Collins and Houlsby, 1997). Within this framework, the free energy is modeled by the strain energy function developed above, while a dissipation function accounts for irreversible (plastic- and possibly viscous-type) effects, and one arrives at a so-called 'generalized standard model'. Alternatively,

one may employ the more classical formulation of Xia et al. (2002) which does not use the thermomechanics approach, but is already developed for finite strains.

The proposed constitutive model has several uses in paper mechanics/physics. One sorely needed application is as input into finite element codes to model response of paper products on larger length scales, such as cardboard boxes, or paper webs on paper machines. Another use is in studies of the effect of formation (i.e. spatial inhomogeneity) of paper on its stochastic, scale dependent response and localization of strains. Such a study, involving a spatial randomization of the strain energy function in the material domain, has recently been pursued in (Ostoja-Starzewski and Castro, 2002; 2003).

Acknowledgements

This material is based upon work supported by the Institute of Paper Science and Technology, the National Science Foundation (Grant CMS-9713764), the US Department of Agriculture (Grant 99-35504-8672), and the Canada Research Chairs program.

References

Aboudi, J., Pindera, M.-J., Arnold, S.M. Higher-order theory for periodic multiphase materials with inelastic phases. Int. J. Plasticity (in press).

Baum, G.A., Habeger, C.C., Fleischman, E.H., 1983. Measurements of the orthotropic elastic constants of paper. The Role of Fundamental Research in Paper Making. Transactions of the Symposium-Cambridge,September 1981, Mechanical Engineering Publications Ltd., pp. 453–478.

Bronkhorst, C.R., Bennett K.A., 2001. Deformation and failure behavior of paper In: Mark, R.E., Habeger, C.C. (Eds.), Handbook of Physical Testing of Paper, Vol 1. Chapter 7. pp. 313–428.

Campbell, J.G., 1961. The in-plane elastic constants of paper. Austral. J. Appl. Sci. 12, 356–357.

Collins, I.F., Houlsby, G.T., 1997. Application of thermomechanical prin-ciples to the modeling of geotechnical materials. Proc. Roy. Soc. Lond. A 453, 1975–2001.

Deng, M., Dodson, C.T.J., 1994. Paper: An Engineered Stochastic Structure. TAPPI Press, Atlanta.

Dłużewski, P., 2000. Anisotropic hyperelasticity based upon general strain measures. J. Elasticity 60, 119–129.

Germain, P., Nguyen Quoc Son, Suquet, P., 1983. Continuum thermodynamics. ASME J. Appl. Mech. 50, 1010–1020.

Houlsby, G.T., Puzrin, A.M., 2000. A thermomechanical framework for constitutive models for rate-independent dissipative materials. Int. J. Plasticity 16, 1017–1047.

Johnson, M.W., Urbanik, T.J., 1984. A nonlinear theory for plastic plates with application to characterizing paper properties. J. Appl. Mech. 51 (3), 146–152.

Maugin, G.A., 1992. The Thermomechanics of Plasticity and Fracture. Cambridge University Press, Cambridge.

Maugin, G.A., 1999. The Thermomechanics of Nonlinear Irreversible Behaviors—an Introduction. World Scientific, Singapore.

Niskanen, K.J., 1993. Strength and fracture of paper. In: Baker,C.F. (Ed.), Products of Paper-making, PIRA 2. pp. 641–725.

Niskanen, K.J., 1998. Paper physics. Paper Science and Technology, Book 16, PI/TAPPI.

Ostoja-Starzewski, M., Stahl, D.C., 2001. Random fiber networks and special elastic orthotropy of paper. J. Elasticity 60, 131–149.

Ostoja-Starzewski, M., 2002. Microstructural randomness versus representative volume element in thermomechanics. ASME J. Appl. Mech. 69, 25–35.

Ostoja-Starzewski, M., Castro, J., 2002. IUTAM Symposium on Micromechanics of Fluid Suspensions and Solid Composites, University of Texas, Austin, TX, 2002.

Ostoja-Starzewski, M., Castro, J., 2003. Random formation, inelastic response and scale effects in paper. Phil. Trans Roy. Soc. Lond. A 361, 965–985.

Ponte Castaneda, P., Suquet, P., 1998. Nonlinear composites. Adv. Appl. Mech. 34, 171–302.

Suhling, J.C., Johnson, M.W., Rowlands, R.E., Gunderson D.E., 1989. Nonlinear elastic constitutive relations for cellulosic materials. In: Mechanics of cellulosic and polymeric materials: Proceedings Joint ASCE/ASME Conference, ASME, pp. 1–15.

Suhling, J.C., 1990. Continuum models for the Mechanical Response of paper and paper composites: past, present, and future. Material Interactions Relevant to Pulp, Paper, and Wood Ind. Proceedings 197, 245–255.

Uesaka, T., Murakami, K., Imamura, R., 1979. Biaxial tensile behavior of paper. Tappi J. 62 (8), 11–114.

Xia, Q.S., Boyce, M.C., Parks, D.M., 2002. A constitutive model for the anisotropic elastic–plastic deformation of paper and paperboard. Int. J. Solids and Struct. 39 (15), 4053–4071.

Ziegler, H., 1983. An Introduction to Thermomechanics. North-Holland, Amsterdam.

Ziegler, H., Wehrli, C., 1987. The derivation of constitutive relations from the free energy and the dissipation functions. Adv. Appl. Mech. 25, 183–238. (Academic Press, New York).